Electronic structure and related properties of Mo–W: a density functional study

2008 J. Phys.: Condens. Matter 20 255208

(http://iopscience.iop.org/0953-8984/20/25/255208)

J. Phys.: Condens. Matter **20** (2008) 255208 (6pp) doi:10.1088/0953-8984/20/25/255208

Electronic structure and related properties of Mo–W: a density functional study

H R Gong[1,3] **and Kyeongjae Cho**[2]

[1] State Key Laboratory of Powder Metallurgy, Central South University, Changsha, Hunan 410083, People's Republic of China
[2] Department of Physics and Electronic Engineering, University of Texas at Dallas, Richardson, TX 75083, USA

E-mail: gonghr@gmail.com

Received 20 March 2008, in final form 21 April 2008
Published 19 May 2008
Online at stacks.iop.org/JPhysCM/20/255208

Abstract

Density functional calculation reveals that Mo and W atoms exhibit a tendency toward layered configurations in bulk Mo–W within the entire composition range at 0 K. Calculation also shows that the electronic structure of bulk Mo is very similar to that of bulk W in terms of the overall density of states, and the Mo–W interaction has a negligible effect on the electronic structure of bulk Mo–W. Moreover, it is discovered that strain has an important effect on the work function, while the changes in work function due to strain are slightly different for Mo and W (110) surfaces. In addition, it is found that Mo surface segregation is energetically favorable for the Mo–W surface within the entire composition range, while it has a negligible effect on the electronic structures of the Mo–W surface.

1. Introduction

During the past few years, metal gate materials for complementary metal-oxide semiconductor (CMOS) technology have been the subject of great research interest to meet the demanding targets set by the International Technology Roadmap for Semiconductors (ITRS) [1]. Replacing polycrystalline silicon gates with metal gates will essentially eliminate effects such as polycrystalline silicon depletion, polycrystalline silicon dopant penetration, and subsequent gate leakage as device miniaturization improves. In addition, metal gates has the advantage of being stable on advanced gate dielectrics, while polycrystalline silicon gates are believed to be thermodynamically unstable on many high-k materials [2, 3].

A major benefit of the traditional polycrystalline silicon gate electrode is the ability to make a Fermi-level adjustment by either donor or acceptor implantation. Tuning of the metal work function, however, is not easily achievable. For bulk devices, the required metal work functions for replacing the conventional n^+- and p^+-polycrystalline silicon gates are about 4 and 5 eV, respectively. Very recently, bilayer metal gate technology has been proven to be a promising way to modulate the work function of metals [3–5].

[3] Author to whom any correspondence should be addressed.

The Mo–W system is being regarded as a good bilayer metal gate candidate for the following reasons. First, the work functions of Mo and W (110) surfaces are close to 5 eV [6], making them suitable for p-MOS applications. Second, the modulation of the Mo–W work function is relatively simple as there is no structural effect on work function in the Mo–W system, and there is only a negligible strain effect on the work function of the Mo–W interfaces. Such a feature of the structural effect is due to the simple Mo–W phase diagram which has no intermetallic phases or crystal structure change below the solidus curve [7, 8], and the negligible strain effect is caused by the very close experimental lattice constants of Mo and W ($a_{\mathrm{Mo}} = 3.13$ and $a_{\mathrm{W}} = 3.16$ Å) and the small difference in the expansion coefficients ($c_{\mathrm{Mo}} = 5.8$–$6.2 \times 10^{-6}\,^{\circ}\mathrm{C}^{-1}$ and $c_W = 4.98 \times 10^{-6}\,^{\circ}\mathrm{C}^{-1}$) [9]. Third, the Mo–W system has attracted much research interest due to its promising application as a metal gate and other aspects [10–14]. Very recently, a first-principles study by the present authors was performed to reveal the Mo–W interface dipole and the effect of the Mo surface segregation on the Mo–W work function [15]. Accordingly, the present study is an extension of this previous work by means of density functional calculations to find out the detailed electronic structure of bulk Mo–W, the strain effect on the work function, and the effect of Mo surface segregation on the electronic structure of Mo–W surfaces.

2. Computational methods

The first-principles calculations are based on the well-established Vienna *ab initio* simulation package (VASP) within the density functional theory (DFT) [16]. Calculations are performed in a plane-wave basis, using the projector-augmented wave (PAW) method [17]. The exchange and correlation potentials are described within the local density approximation (LDA) of Perdew and Zunger [18], and the cutoff energies are 300 and 450 eV for the plane-wave basis and augmentation charge, respectively. It should be noted that, in comparison with the generalized-gradient approximation (GGA), the LDA provides a better description of the work function for transition metals [19]. In each calculation, periodic boundary conditions are added in three directions of the unit cell. During the relaxation calculation, the energy criteria are 0.01 and 0.1 meV for electronic and ionic relaxations, respectively, while for the calculation of the density of states (DOS), the energy self-consistency is achieved within 0.001 meV. After each DOS calculation, the work function is derived as the difference between the vacuum and Fermi levels, and the vacuum level is determined as the electrostatic potential at a sufficient distance from the surface [20].

At the early stage of this study, we did a series of test calculations, such as the k-point convergence test, the number of surface layers test, and the number of vacuum layers test. As a result, the Gamma centered k-grid is adopted for all the calculations, i.e. $11 \times 11 \times 11$ and $13 \times 13 \times 13$ for the bulk relaxation and bulk DOS, respectively, and $9 \times 9 \times 1$ and $11 \times 11 \times 1$ for the surface relaxation and surface DOS, respectively. For k-space integration, the temperature-smearing method of Methfessel–Paxton [21] is used for the relaxation calculation and the modified tetrahedron method of Blöchl–Jepsen–Andersen [22] is used for the DOS calculation. After the layer test, a 1×1 surface unit cell with nine surface layers and seven vacuum layers is used for the strain effect calculation, and a 2×2 surface unit cell with nine surface layers and eleven vacuum layers is considered for the alloy surface calculation.

Before the surface calculation, the bulk calculation with a $2 \times 2 \times 2$ unit cell of the bcc structure was done for the Mo–W system within the entire composition range. At each composition, various atomic configurations are calculated, to find out the optimized crystal structure corresponding to the lowest total energy. In addition, for each configuration at a given composition, the atoms are fully relaxed to find out the optimized lattice constant corresponding to the lowest total energy. As a result, the optimized atomic configuration with the optimized lattice constant from the bulk calculation is used for the corresponding alloy surface calculation.

In the present study, the surface calculation is focused on the bcc (110) surface orientation due to its high stability, and basically there are two kinds of surface calculations to probe strain and alloy effects. For the strain effect calculations, the area of the surface unit cell is increased (decreased) within a certain range, corresponding to a certain amount of tensile strain (compressive strain). The alloy surface calculations are performed within the entire composition range of the Mo–W system, and at each composition two cases are considered, i.e. with and without the surface segregation of the Mo atoms.

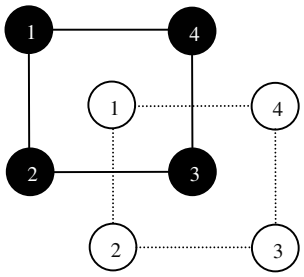

Figure 1. Schematic atomic positions in the bcc bulk with a unit cell of $2 \times 2 \times 2$. Filled and unfilled circles represent the atoms in the first and second (001) layers, respectively.

3. Results and discussion

3.1. Electronic structures of bulk Mo–W

To find out the Mo–W interaction at the electronic scale, a $2 \times 2 \times 2$ unit cell with the bcc structure is selected for the bulk calculations and 17 compositions (including pure Mo and W) are chosen with an equal interval within the entire composition range. At each composition, all possible atomic configurations of Mo and W atoms are fully relaxed, and the atomic configuration with the lowest total energy among all these configurations is therefore regarded as the optimized crystal structure for the bulk Mo–W at this composition [23]. For the crystal structure, figure 1 shows a schematic picture of the atomic positions in the first and second (001) layers of the bcc bulk, and each atom is numbered to provide a clear description of various atomic configurations. It should be pointed out that the $2 \times 2 \times 2$ unit cell with the periodic boundary condition was used to reveal the mixing behavior of the bcc Nb–W system from first-principles calculations [24].

After the calculation, table 1 displays the structural properties of some bulk Mo–W with several selected atomic configurations, which are expressed by the combination of the numbers of solute atoms (Mo or W) shown in figure 1. For instance, the atomic configuration of 1–2–4–3 for bulk $Mo_{75}W_{25}$ means that the four W atoms are at the 1, 2, 4, and 3 positions in the first, second, third, and fourth (001) layers, respectively. From this table, one can see that the lattice constants of bulk Mo–W from the present first-principles calculation are in good agreement with the available experimental data [15]. It can also be observed that the atomic configurations of 0-0-1234-0, 0-1234-0-1234, and 0-0-1234-0 are the optimized structures corresponding to the lowest total energies for bulk $Mo_{75}W_{25}$, $Mo_{50}W_{50}$, and $Mo_{25}W_{75}$, respectively. That is to say, the Mo and W atoms exhibit a tendency to become layered atomic configurations in bulk Mo–W within the entire composition range at 0 K, which is different from the Mo–W solid solutions over the entire composition range found experimentally at high temperature [25].

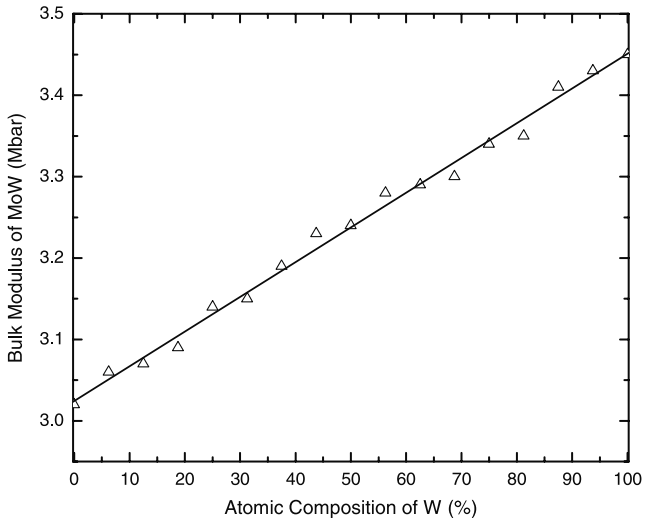

Figure 2. Bulk modulus (Mbar) of bulk Mo–W alloy versus composition.

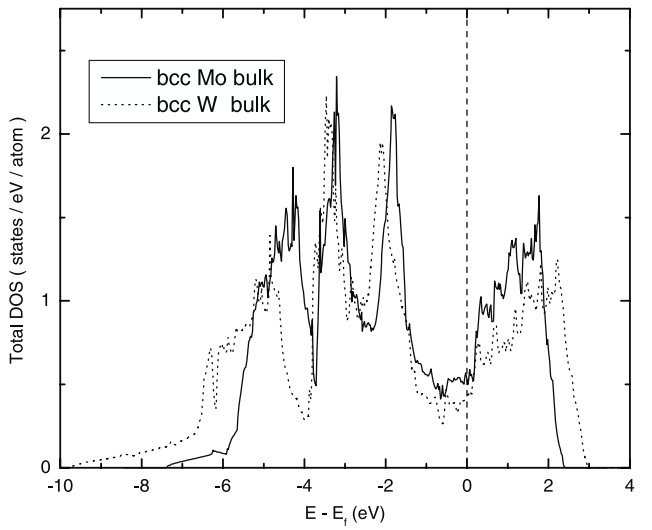

Figure 3. Total density of states (DOS) of bcc-based bulk Mo and W, respectively.

Table 1. Structural properties of several bulk Mo–W compositions with a unit cell of $2 \times 2 \times 2$. a is the lattice constant and ΔE is the structural energy difference.

	a (Å)			ΔE
Bulk	This work	Exp.[a]	Atomic configuration[b]	(eV/unit cell)
$Mo_{75}W_{25}$	3.11		**0-0-1234-0**	0
			3-0-124-0	0.00460
			24-0-13-0	0.00656
			1-2-4-3	0.04190
$Mo_{50}W_{50}$	3.115	3.15	**0-1234-0-1234**	0
			1-234-1-234	0.10420
			12-34-12-34	0.13146
			24-24-13-13	0.15255
$Mo_{25}W_{75}$	3.12		**0-0-1234-0**	0
			3-0-124-0	0.00616
			1-1-1-1	0.03389
			24-0-13-0	0.04656
Mo	3.10	3.14		
W	3.13	3.16		

[a] Reference [10].
[b] See figure 1 and the text for details.

The bulk modulus of bulk Mo–W is also calculated within the entire composition range and the results are shown in figure 2. It can be seen that the bulk moduli of pure Mo and W are 3.02 and 3.45 Mbar, respectively, which is compatible with the corresponding experimental values of 2.72 and 3.23 Mbar [26], respectively. This implies that the LDA in the present study gives a slightly bigger bulk modulus than the experimental value. It can also be observed that composition has an almost linear effect on the Mo–W bulk modulus, implying that the electronegativities of Mo and W atoms are almost identical [15].

To find out the intrinsic mechanism of the Mo–W interaction, the electronic structure of bulk Mo–W is derived at each composition within the entire composition range. As a typical example, figure 3 shows the comparison of the total DOS for pure bulk Mo and W, respectively. It can be observed from this figure that both DOSs are similar in terms of the shape and height of the DOS peaks, while the bandwidth for bulk Mo is smaller than for bulk W. In particular, both Fermi levels are located in the pseudogap region with a clear separation of the bonding and antibonding states, and the DOS at the Fermi level of bulk Mo is very close to that of bulk W, suggesting that the chemical activities of bulk Mo and W are almost identical. It should be pointed out that the almost equal DOSs at the Fermi energy are consistent with the results of Mo–W interface dipole calculations [15] and could also give a reasonable explanation for the almost equal loss of electrons of Mo and W interface atoms revealed in a previous study [15]. Moreover, it is of interest to see that the electronic structures of bulk Mo and W from the present PAW calculation are quite similar to those from the tight-binding linear muffin-tin orbital (TB-LMTO) calculation [11], while the small difference between the DOSs would probably be due to the different theoretical methods used in these two studies.

In addition, figure 4 shows a comparison of the DOS of bulk $Mo_{50}W_{50}$ as well as the mechanical mixture of 50 at.% Mo and 50 at.% W (without any Mo–W interaction). It can be seen that there is only a very small difference between these two curves in figure 4, which means that the Mo–W interaction has a negligible effect on the electronic structure of bulk $Mo_{50}W_{50}$. It should be noted that such a negligible effect of the Mo–W interaction on the DOS could give a reasonable explanation for the almost linear Mo–W work function with alloy composition reported before [15] as well as for the almost linear change of bulk modulus with alloy composition in the present study. Interestingly, it should be pointed out that the electronic structure of bulk $Mo_{50}W_{50}$ from the present PAW calculation is also similar to that from the TB-LMTO method in the literature [11].

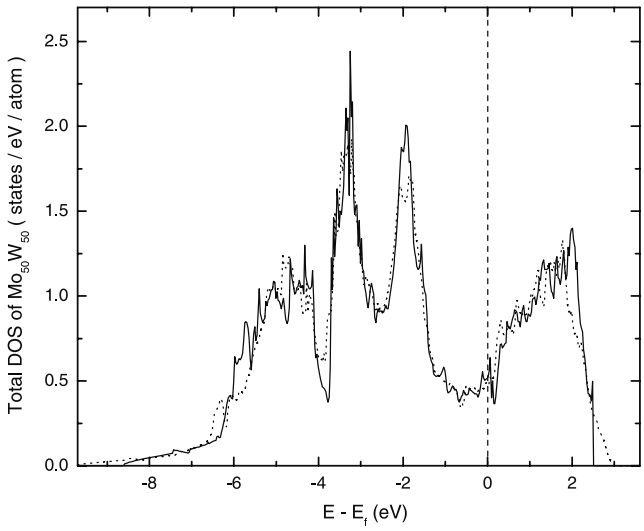

Figure 4. Comparison of total densities of states (DOS). The solid line is for bulk $Mo_{50}W_{50}$ and the dotted line is for the mechanical mixture of 50 at.% Mo and 50 at.% W.

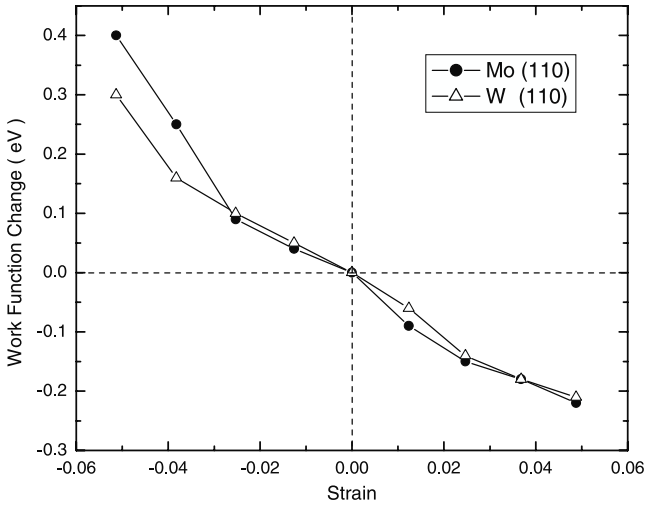

Figure 5. Work function change with respect to strain for the Mo and W (110) surfaces, respectively.

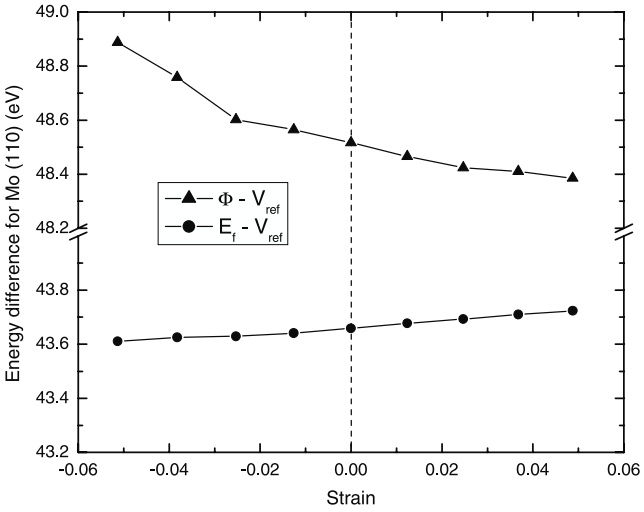

Figure 6. Variation of the two contributions to the work function (see text) for a Mo (110) surface with strain.

3.2. Strain effect on work function

It is commonly believed that some kind of strain will appear during the actual gate integration, and such strain will undergo certain changes thereafter. It is therefore important to find out, in a qualitative and quantitative way, the effect of strain on electronic structure and work function of the metal gate electrode. In this respect, first-principles method calculations based on DFT have been proven suitable for studying the electrical properties of metals and alloys, and we hope that the present first-principles study of the strain effect could thus provide some guide to the control of the work function in actual metal gate electrodes.

For the strain effect calculation, the area of the surface unit cell is increased (decreased) within a certain range, corresponding to a certain amount of tensile strain (compressive strain). Accordingly, figure 5 shows the change in work function of Mo and W (110) surfaces with respect to strain. One can see that the work function increases (decreases) when the surface is compressed (expanded). It can also be noted that the change in work function due to strain is slightly different for Mo and W (110) surfaces, i.e. in the strain range of −0.05–0.05, the work function change is 0.4 to −0.22 eV for Mo, while it is 0.31 to −0.21 eV for W. It should be pointed out that the general trends of the strain effect on work function from first-principles calculations are in good agreement with those from experimental studies as well as semi-empirical models found in the literature [27–30].

We now try to identify the mechanism of the above change in work function due to strain in the Mo–W system. According to the definition, the work function (WF) is the difference between the vacuum (ϕ) and the Fermi levels (E_f). If V_{ref} is defined as the average electrostatic potential at each ion over the core and this term is added to the formula, the WF can then be described as the difference between the following two terms:

$$\mathrm{WF} = \phi - E_f = (\phi - V_{ref}) - (E_f - V_{ref}). \quad (1)$$

The two quantities in parentheses are known as surface dipole and bulk electronic structure terms. Accordingly, figure 6 shows these two terms as functions of strain for the Mo (110) surface. One can see clearly from this figure that the surface dipole term increases (decreases) with increased compression (expansion), while the bulk electronic structure term decreases (increases) with increased compression (expansion). That is to say, the effects of these two terms under strain are in the same direction, i.e. both surface dipole and bulk electronic structure increase (decrease) the work function with increased compression (expansion), and the overall effects on work function can be seen in figure 5. Additionally, the change in surface energy under strain is also calculated and summarized in figure 7. It is of interest to see that the surface energy increases under strain, and this increase for the Mo (110) surface is quite similar to that of the W (110) surface.

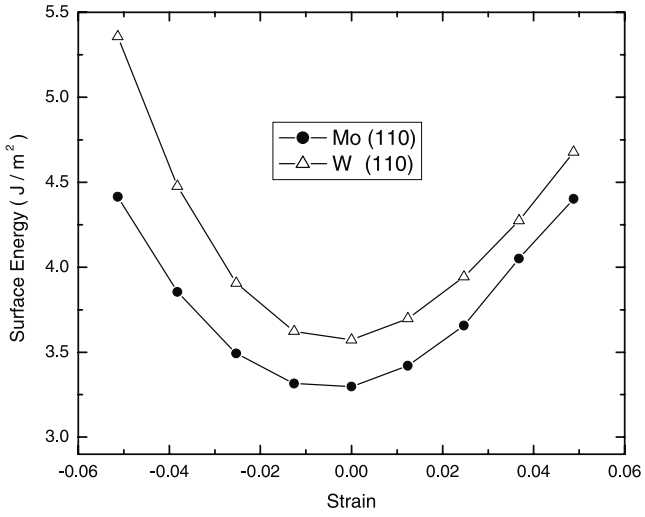

Figure 7. Change in surface energy with respect to strain for the Mo and W (110) surfaces, respectively.

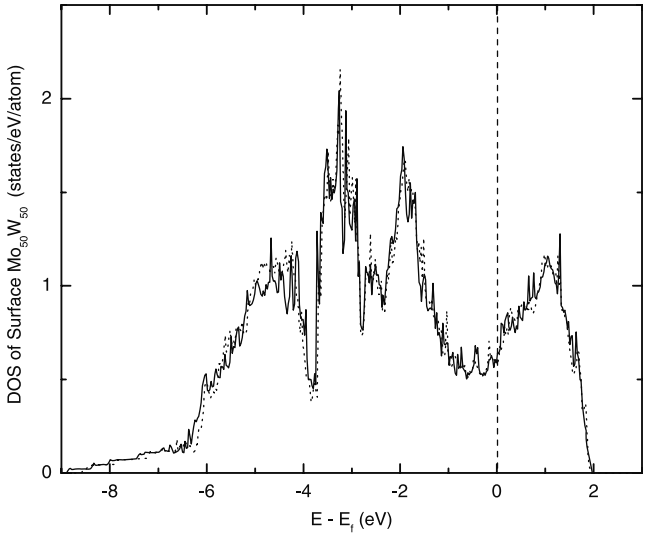

Figure 8. Effect of surface segregation on the DOS. The solid line and the dotted line are for the $Mo_{50}W_{50}$ surface with and without Mo surface segregation, respectively.

3.3. Effect of Mo surface segregation on the electronic structure of Mo–W

As reported both experimentally and theoretically in the literature, the Mo atoms in the Mo–W system have a tendency to segregate at the surface [31, 32]. It was revealed in our recent paper [15] that the Mo surface segregation has an important effect on reducing the work function of Mo–W alloy within the entire composition range, and that the work function of the Mo–W surface under surface segregation becomes relatively stable in the composition range of 0–70 at.% W. In the present study, it is therefore of interest to find out the effect of Mo surface segregation on the electronic structure and related properties of the Mo–W surface.

For the Mo–W surface calculation at each composition, the optimized bulk Mo–W structure revealed in section 3.1 is used as the starting structure for surface relaxation, and the relaxed configuration is then regarded as the corresponding Mo–W (110) surface without Mo surface segregation. To calculate the Mo surface segregation, the Mo atoms in the optimized bulk Mo–W structure are artificially put to the surface before the surface relaxation, and the atomic configuration with the densest Mo atoms in the surface region is regarded as the Mo–W (110) surface with Mo surface segregation. Accordingly, the surface segregation energy of the Mo atoms is calculated as the energy difference between the relaxed Mo–W (110) surfaces with and without Mo surface segregation.

The present first-principles calculation reveals that Mo surface segregation has a negligible effect on the electronic structure of the Mo–W surface within the entire composition range. As a typical example, figure 8 shows a comparison of the DOS of a $Mo_{50}W_{50}$ (110) surface with and without Mo surface segregation. It can be noticed from the figure that these DOS curves for $Mo_{50}W_{50}$ are very similar to each other, implying that the effect of Mo surface segregation on the electronic structure of Mo–W surfaces can be nearly disregarded. As discussed before, Mo surface segregation has

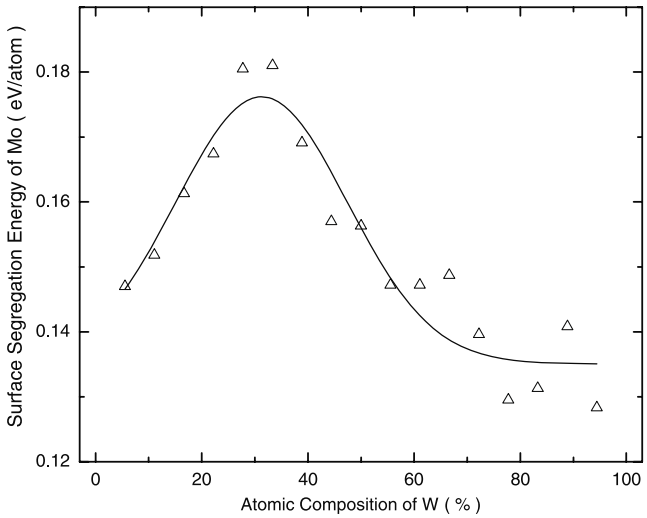

Figure 9. Surface segregation energy of Mo versus composition.

the important effect of reducing the work function of Mo–W surfaces, and the work function could be expressed as the difference between the two terms shown in equation (1), i.e. the surface dipole term and the bulk electronic structure term. Considering the above statements together, the negligible effect of Mo surface segregation on surface electronic structure suggests that Mo surface segregation should probably have a strong effect on the surface dipole of Mo–W surfaces.

Finally, we consider the thermodynamics of Mo surface segregation. At first, the segregation energy of Mo atoms to the surface is calculated within the entire composition range and the results are displayed in figure 9. One sees from this figure that the segregation energy of Mo is in the range of 0.13–0.18 eV atom^{-1} with a maximum at a composition of about 30 at.% W. Thermodynamically, the above observation means that the segregation of Mo atoms to the surface is energetically favored within the entire composition range and

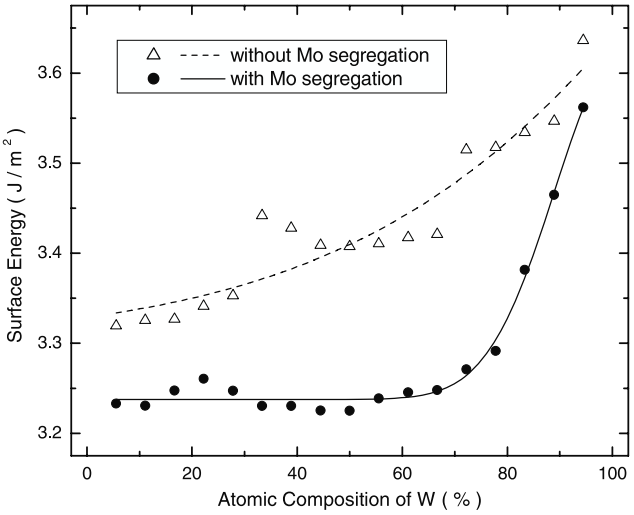

Figure 10. Surface energy of the Mo–W surface with and without Mo surface segregation, respectively.

it seems more favorable for the Mo atoms to segregate to the surface within the W composition range of 20–40 at.%. In addition, the surface energy of the Mo–W (110) surface is also calculated and shown in figure 10. It can be seen that the surface segregation has a strong effect on reducing the surface energy of the Mo–W (110) surface within the entire composition range, and it is of interest to see that relatively stable surface energies could be obtained when the Mo–W surface with Mo surface segregation is in the composition range of 0–60 at.% W.

4. Concluding remarks

In the present study, calculations based on DFT have been performed to investigate the effect of Mo–W interaction, strain, and surface segregation on the electronic structure and related properties of the Mo–W metal gate system. It is revealed that the Mo and W atoms have a tendency toward layered configurations in bulk Mo–W within the entire composition range, and that the effect of the Mo–W interaction on the electronic structure of bulk Mo–W could be nearly disregarded. It is also shown that strain has an important effect on work function, while Mo surface segregation has only a negligible effect on the electronic structure of the Mo–W surface.

Acknowledgments

This research work is supported by the Creative research group of the National Natural Science Foundation of China (grant no. 50721003).

References

[1] The International Technology Roadmap for Semiconductors. Available from: http://public.itrs.net
[2] Lin R, Lu Q, Ranade P, King T J and Hu C 2002 *IEEE Electron Devices Lett.* **23** 49
[3] Efavi J K, Mollenhauer T, Wahlbrink T, Gottlob H D B, Lemme M C and Kurz H 2005 *J. Mater. Sci. Mater. Electron.* **16** 433
[4] Polishchuk I, Ranade P, King T J and Hu C 2001 *IEEE Electron Devices Lett.* **22** 444
[5] Li T L, Hu C H, Ho W L, Wang H C H and Chang C Y 2005 *IEEE Trans. Electron Devices* **52** 1172
[6] Michaelson H B 1977 *J. Appl. Phys.* **48** 4729
[7] de Boer F R, Boom R, Mattens W C M, Miedema A R and Niessen A K 1989 *Cohesion in Metals: Transition Metal Alloys* (Amsterdam: North-Holland)
[8] Villars P and Calvert L D 1991 *Pearson's Handbook of Crystallographic Data for Intermetallic Phases* vol 4 (Materials Park, OH: The Materials Information Society)
[9] Pearson W B 1958 *A Handbook of Lattice Spacings and Structures of Metal and Alloys* (Belfast: Pergamon Press)
[10] Jun S I, Rack P D, McKnight T E, Melechko A V and Simpson M L 2005 *J. Appl. Phys.* **97** 054906
[11] Turchi P E A, Drchal V, Kudrnovský J, Colinet C, Kaufman L and Liu Z K 2005 *Phys. Rev.* B **71** 094206
[12] Li G Y, Xu J H, Zhang L Q, Wu L and Gu M Y 2001 *J. Vac. Sci. Technol.* B **19** 94
[13] Svedberg E B, Birch J, Ivanov I, Münger E P and Sundgren J E 1998 *J. Vac. Sci. Technol.* A **16** 633
[14] Vill M A, Rek Z U, Yalisove S M and Bilello J C 1995 *J. Appl. Phys.* **78** 3812
[15] Gong H R and Cho K 2007 *Appl. Phys. Lett.* **91** 092106
[16] Kresse G and Hafner J 1993 *Phys. Rev.* B **47** 558
[17] Kresse G and Joubert J 1999 *Phys. Rev.* B **59** 1758
[18] Perdew J and Zunger A 1981 *Phys. Rev.* B **23** 5048
[19] Park S, Colombo L, Nishi Y and Cho K 2005 *Appl. Phys. Lett.* **86** 073118
[20] Lang N D and Kohn W 1971 *Phys. Rev.* B **3** 1215
[21] Methfessel M and Paxton A T 1989 *Phys. Rev.* B **40** 3616
[22] Blöchl P E, Jepsen O and Andersen O K 1994 *Phys. Rev.* B **49** 16223
[23] Blum V and Zunger A 2005 *Phys. Rev.* B **72** 020104
[24] Gong H R, Nishi Y and Cho K 2008 *J. Appl. Phys.* **103** 043702
[25] Massalski T B 1990 *Binary Alloy Phase Diagrams* (Metals Park, OH: ASM International)
[26] Mehl M J and Papaconstantopoulos D A 1996 *Phys. Rev.* B **54** 4519
[27] Li W, Cai M, Wang Y and Yu S 2006 *Scr. Mater.* **54** 921
[28] Li W and Li D Y 2005 *Appl. Surf. Sci.* **240** 388
[29] Kiejna A and Pogosov V V 2000 *Phys. Rev.* B **62** 10445
[30] Loskutov S V 2005 *Surf. Sci.* **585** L166
[31] Dawson P T and Petrone S A 1981 *J. Vac. Technol.* **18** 529
[32] Ouannasser S, Dreyssé H and Wille L T 1995 *Solid State Commun.* **96** 177
Ouannasser S, Dreyssé H and Wille L T 2004 *Surf. Sci.* **553** 30